


CERTIFICATE

It is certified that the work contained in the thesis titled "Electrically stimulated sodium potassium niobate [$\text{Na}_x\text{K}_{1-x}\text{NbO}_3$ ($x = 0.2 - 0.8$), NKN] piezo-bioceramics toward the development of electro-active prosthetic orthopedic implant" by DEEPAK KHARE has been carried out under my supervision and that this work has not been submitted elsewhere for a degree.

It is further certified that the student has fulfilled all the requirements of Comprehensive examination, Candidacy and SOTA for the award of Ph.D. Degree.


Dr. Ashutosh Kumar Dubey

(Supervisor)
Associate Professor
Department of Ceramic Engineering
Department of Ceramic Engineering
सेरामिक अभियान्त्रकी विभाग
Indian Institute of Technology (B.H.U.)
IIT (BHU) Varanasi
भारतीय प्रौद्योगिकी संस्थान (काठहोवाँ) (वि०)
Varanasi-221005/वाराणसी-221005

DECLARATION BY THE CANDIDATE

I, "Deepak Khare", certify that the work embodied in this thesis is my own bona fide work and carried out by me under the supervision of "Dr. Ashutosh Kumar Dubey, Associate Professor" for a period of 5 years and 10 months from "July, 2016" to "May, 2022", at the "Department of Ceramic Engineering", Indian Institute of Technology (BHU), Varanasi. The matter embodied in this thesis has not been submitted for the award of any other degree/diploma. I declare that I have faithfully acknowledged and given credits to the research workers wherever their works have been cited in my work in this thesis. I further declare that I have not willfully copied any other's work, paragraphs, text, data, results, etc., reported in journals, books, magazines, reports dissertations, theses, etc., or available at websites and have not included them in this thesis and have not cited as my own work.

Date : 28/5/2022

Place: Varanasi

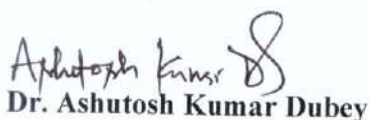


(Deepak Khare)

Candidate

CERTIFICATE BY THE SUPERVISOR

It is certified that the above statement made by the student is correct to the best of my/our knowledge.


Dr. Ashutosh Kumar Dubey

Associate Professor
Department of Ceramic Engineering
सैरामिक अभियान्त्रिकी विभाग
(Supervisor)
Indian Institute of Technology (B.H.U.)
भारतीय प्रौद्योगिकी संस्थान (का०हि०वि०वि०)
Varanasi-221005/ वाराणसी-221005


Head of Ceramic Engineering Department
HEAD/ विभागाध्यक्ष
Department of Ceramic Engineering
सैरामिक अभियान्त्रिकी विभाग
Indian Institute of Technology (B.H.U.)
भारतीय प्रौद्योगिकी संस्थान (का०हि०वि०वि०)
Varanasi-221005/ वाराणसी-221005

COPYRIGHT TRANSFER CERTIFICATE

Title of the Thesis: “Electrically stimulated sodium potassium niobate [$\text{Na}_x\text{K}_{1-x}\text{NbO}_3$ ($x = 0.2 - 0.8$), NKN] piezo-bioceramics toward the development of electro-active prosthetic orthopedic implant”

Name of the Student: **Deepak Khare**

Copyright Transfer

The undersigned hereby assigns to the Institute of Technology (Banaras Hindu University) Varanasi all rights under copyright that may exist in and for the above thesis submitted for the award of the degree of “Doctor of Philosophy”.

Date: 20/5/2022

Place: Varanasi



Deepak Khare

Note: However, the author may reproduce or authorize others to reproduce material extracted verbatim from the thesis or derivative of the thesis for author's personal use provided that the source and the Institute's copyright notice are indicated.

Acknowledgement

I am deeply grateful to my supervisor **Dr. Ashutosh Kumar Dubey**, for giving me the confidence to explore my research interests. His immense knowledge in the field of materials science and the way of sharing it always pushed me to know more deeply and fundamentally about the field. I must gratefully acknowledge his constant encouragement and help in different ways to complete my thesis successfully.

I would also like to thank my research evaluation committee members, **Dr. Sanjeev Kumar Mahto** and **Dr. Imteyaz Ahmad** for their valuable advice towards the present work. I would also like to thank **Dr. Vinay Kumar Singh** Heads and Professors in the Department of Ceramic Engineering, IIT(BHU) for providing the necessary resources to enable me to carry out my research work.

I would like to thank my friends, colleagues and labmates **Dr. Abhinav Saxena** for helping me during experiments, **Ms. Priya Singh** for sharing with me some key knowledge on needful software and **Ms. Urvashi Kesarwani** for creating a work friendly environment in the lab.

I would also like to thank my other friends and colleagues such as Harsh Jain, Kuntal Kumar Das, Mukesh Shuthar, Priya Singh, Nitesh Malan, Rahul Kumar, Pradeep Sandeep Maurya, Anurag Kumar for making my life memorable at the campus of IIT (BHU). I would also like to thanks to staff members of the department Mr. Bhagmal Singh, Mr. Shailendra, Mr. Pawan Kumar, Mr. Ashish Tripathi for helping me in experimental and paper work.

I would like to express my special gratefulness to my parents **Mr. Hanuman Prasad Khare** and **Mrs. Manju Khare** for their unconditional support, both financially and emotionally throughout my research work. I express my deep sense of gratitude to my younger brother **Mr. Shobhit Khare**, elder sister **Mrs. Jyoti Khare** and brother in law

Ashish Srivastava for their constant encouragement, which gave me courage and confidence to materialize my dream.

I would also like to thank **GOD** the almighty for giving me the strength to remain on the path to success.

Date: 28/5/2022

Place: IIT (BHU) Varanasi



(Deepak Khare)

DEDICATED
to
My Beloved Parents

Contents

Table of contents

List of Publications

List of Figures

List of Tables

Chapter 1	Introduction	1-17
1.1	Background and motivation	1
1.2	The electroactive response of natural bone	2
1.3.	Overview of piezoelectric bioceramics	5
1.4	Surface polarization and external electrical stimulation induced cellular response	6
1.5	Surface charge induced antibacterial response	7
1.6	Objectives	8
1.7	Outlines for the thesis	8
Chapter 2	Literature Review	18-102
2.1	Introduction	18
2.2	Piezoelectric biomaterials	25
2.3	Processing-related challenges for piezoelectric NKN-based ceramics system	30
2.4	Addressing the processing concerns for piezoelectric NKN-based ceramics	35
2.4.1	Conventional processing routes	37
2.4.2	Advanced processing routes	38
2.4.3	Chemical modification	42
2.5	Piezoelectricity and biocompatibility	46

2.5.1	Origin of biomineralization and cytocompatibility	46
2.5.2	Origin of bone healing	50
2.5.3	Influence of electrical stimulation on the biological response	53
2.5.4	Biomaterials-based perspective	54
2.5.4.1	NKN-based piezoelectric ceramics	54
2.5.4.2	Other piezoelectric ceramics	56
2.5.4.3	Piezoelectric polymers	60
2.6	Surface charge polarization induced antibacterial response	62
2.6.1	Bacterial infection	62
2.6.2	Influence of surface charge and other external stimuli on bacteria	62
Chapter 3	Experimental Design (Materials and methods)	103-130
3.1	Synthesis	103
3.1.1	Synthesis of sodium potassium niobates [$\text{Na}_x\text{K}_{1-x}\text{NbO}_3$ ($x = 0.2 - 0.8$), NKN]	103
3.1.2	Synthesis of hydroxyapatite (HA)	104
3.2	Consolidation of synthesized $\text{Na}_x\text{K}_{(1-x)}\text{NbO}_3$ and HA powders	105
3.3	Characterization	106
3.3.1	X-ray diffraction analyses	106
3.3.2	Fourier transform infrared (FTIR) spectroscopy	108
3.3.3	Microstructural analyses	108
3.4	Densification and mechanical property measurement	108
3.5	Ion leaching study of NKN samples in simulated body fluid (SBF)	109

3.6	Polarization treatment of the samples	109
3.7	Surface charge measurement	110
3.8	X-ray photoelectron spectroscopy (XPS)	111
3.9	Physical characterization (Contact angle measurement)	111
3.10	Cellular response	111
3.10.1	Quantitative analyses	112
3.10.1.1	MTT assay	112
3.10.1.2	Alkaline phosphatase (ALP) activity	113
3.10.2	Morphological analyses of adhered cells	114
3.10.3	Intracellular Ca ²⁺ ions measurement	114
3.11	Antibacterial response	116
3.11.1	Quantitative analyses	116
3.11.1.1	MTT assay	116
3.11.2	Qualitative analyses	117
3.11.2.1	Fluorescence imaging	117
3.11.2.2	Disk diffusion method	117
3.12	<i>In vivo</i> assessment of systematic toxicity of nano-sized NKN powder	118
3.12.1	Nano-sized powder preparation	118
3.12.2	Characterization of nano-powders	119
3.12.3	Preparation of eluate solution	119
3.12.4	Cell - NKN nanoparticles interaction	119
3.12.5	Animal study	121
3.12.5.1	General observation	122
3.12.5.2	Biochemical assay for serum assessment	123
3.12.5.3	Inflammatory test with organs	124

3.12.5.3.1	Inflammatory cytokines profiling	124
3.12.5.3.2	Histopathological analyses	125
3.12.6	Statistical analyses	125
Chapter 4	Combined effect of surface polarization and external electrical stimulation towards accelerated osteogenic response of $\text{Na}_x\text{K}_{1-x}\text{NbO}_3$ ($x = 0.2 - 0.8$) piezobioceramics	131-172
4.1	Phase evolution	132
4.1.1	XRD analyses	132
4.1.2	Crystallite size and strain measurement	135
4.1.3	Fourier transform infrared (FTIR) spectroscopy	138
4.2	Microstructural analysis	139
4.3	The densification and mechanical property (Vicker's Hardness) measurement	141
4.4	Leaching behavior of NKN pellets in biological fluid (SBF)	142
4.5	Charge measurement	143
4.6	X-ray photoelectron spectroscopy (XPS) analyses	144
4.7	Contact angle measurement	147
4.8	Cellular response	148
4.8.1	Polarization induced early-stage cell adhesion	148
4.8.2	Combined effect of surface polarization and dynamic electrical stimulation	151
4.8.2.1	MTT assay	151
4.8.2.2	Alkaline phosphatase (ALP) activity assessment	155
4.8.2.3	Morphological analyses of adhered cells	158
4.8.2.4	Intracellular Ca^{2+} measurement	160
4.9	Discussion	162

Chapter 5	Antibacterial response of surface polarized and compositionally modified biocompatible $\text{Na}_x\text{K}_{1-x}\text{NbO}_3$ ($x = 0.2 - 0.8$) ceramics	173-200
5.1	Quantitative antibacterial analyses or MTT assay	173
5.2	Qualitative analyses	178
5.2.1	Live/ dead assay	178
5.2.2	Disk diffusion method of colony counting	179
5.3	Enzymatic activity for reactive oxygen species (ROS) measurement	182
5.3.1	SOD assay	182
5.3.2	Catalase assay	185
5.3.3	ROS induced damaged protein estimation	187
5.3.4	LPO assay	189
Chapter 6	An <i>in vivo</i> toxicity assessment of piezoelectric $\text{Na}_x\text{K}_{1-x}\text{NbO}_3$ ($x = 0.2 - 0.8$) nanoparticulates towards bone tissue engineering approach	201-236
6.1	Characterization of $\text{Na}_x\text{K}_{1-x}\text{NbO}_3$ nanoparticulates	201
6.2	Morphological analyses	202
6.3	Initial screening of toxicity (Cell culture study)	203
6.4	Animal study	206
6.4.1	General observations	206
6.4.2	Effect of intra-articular injection of N1, N2 and N3 compositions on the body weight	207
6.4.3	Biochemical assay	208
6.4.4	Inflammatory cytokines analyses	210
6.4.5	Histopathological analyses (hematoxylin and eosin staining)	212
Chapter 7	Conclusion and scope for the future work	237-241
	Conclusions	237
	Future scope	240

List of figures

- Fig. 2.1 : *Stress generated electrical charges in natural bone and piezoelectric biomaterials induced endogenous cellular potential and bone formation. (A) Schematic demonstration of the generation of aligned dipoles or surface charge on piezoelectric ceramic (BaTiO_3) and polymer (PLLA) with the application of mechanical stress, similar to human bone. (B) Stress generated surface electrical charge on the circumference of human femur. (C) Schematic illustration of the generation of surface electrical charge on strained piezoelectric material and resulting hyper-polarization/ depolarization of cellular membrane. (D) Schematic representation of built-in electric field between positively charged nanocomposite and negatively charged bone wall, which enhances the osseointegration. (E) Histological evidences demonstrating significant neobone formation on the positively charged implant, when compared to negatively charged and uncharged implant (Yellow dotted block: implant-tissue interface, NB: nascent bone, FT: fibrous tissue, BFO: BiFeO_3 , STO: SrTiO_3).* 21
- Fig. 2.2 : *Piezoelectric potential generated from natural bone during regular physiological activity. [(A), (B) and (C)] PVDF based piezoelectric sensors (PS) as detectors of human activity in terms of piezoelectricity induced voltage output. [D] P(VDF-TrFE) based piezo-polymers (nanogenerator) implanted in the thigh of Sprague Dawley rat, mimicking piezoelectric potential generation during the regular activity. (A) PS nanocomposite, fabricated with PVDF/ SiO_2 coated NiO assembled with gloves to determine the piezoelectric voltage output variation during stretching and bending movement of index, middle and ring fingers. (B) A PS nanocomposite with tetrapod ZnO/ PVDF/ polyester fabric, attached with elbow, to evaluate the amount of voltage output during bending and release. (C) A PS fabricated with PVDF/ graphene in polyester fabric attached with marked region to determine the voltage output variation during running. (D) Electrospun P(VDF-TrFE) nanoscaffold implanted in the thigh of Sprague Dawley rat. The leg of rat was pulled up and released through a motor (bottom-right) and resulting variation in current output are shown (top-right) during pulling and releasing. The current and voltage output are also shown in bottom-left and bottom-middle graph, respectively in the pulling condition of rat's leg.* 23
- Fig. 2.3 : *Schematic illustrating the temperature dependent phase transformations (a) In $\text{Na}_{0.5}\text{K}_{0.5}\text{NbO}_3$ and (b) In BaTiO_3 ceramics.* 25

- Fig. 2.4 : Classification of various crystal classes on the basis of the center of symmetry with reference to piezoelectricity, pyroelectricity and ferroelectricity. 29
- Fig. 2.5 : (a). Phase diagram of $\text{KNbO}_3\text{-NaNbO}_3$ solid solution, where P and F denote the paraelectric and ferroelectric phases, respectively. R, O, T and C indicate rhombohedral, monoclinic / orthorhombic, tetragonal and cubic phases, respectively. In $\text{Na}_x\text{K}_{1-x}\text{NbO}_3$, the morphotropic phase boundary (MPB) at $x = 0.5$ distinguishes two orthorhombic and two tetragonal phases. Below Curie temperature, polymorphs like tetragonal - monoclinic / orthorhombic and monoclinic / orthorhombic - rhombohedral coexist at about 200°C and -160°C , respectively. (b) Polymorphic phase transformation (PPT): tetragonal to monoclinic / orthorhombic (polymorphs) phase transformation temperature of NKN can be shifted to room temperature by chemical modification, indicating the dependency of PPT on composition as well as temperature, (c) Morphotropic phase boundary (MPB): Coexistence of rhombohedral and tetragonal phases at a certain composition. 32
- Fig. 2.6 : Schematic representing key issues, associated with the processing of stoichiometric NKN 35
- Fig. 2.7 : Surface polarization induced bioactivity and cellular response, in vitro and in vitro. Polarized surfaces of piezoelectric materials promote the adsorption of apatite ions (Ca^{2+} , HPO_4^{2-}) or proteins and cell adhesion, which consequently influence the hard tissue regeneration. 48
- Fig. 2.8 : Schematic illustration of the effect of mechanical stimulation on cell metabolism through intracellular electrical signal transduction, leading to activation of mechanoreceptors. Electromechanical signals facilitate outside-in Ca^{2+} ions influx through the opening of voltage gated Ca^{2+} channels (VGCC) and stretch activated calcium channels (SACC). Consequently, intracellular ions increase which activate the calmodulated protein and calcineurin. These calcium activated calcineurin dephosphorylates the phosphorylated nuclear factor of activated cells (NF-AT) and shifts towards the nucleus, where it executes gene transcription. Mechanically stimulated membrane receptors open up receptor channels and permit intracellular Ca^{++} ions from endoplasmic reticulum calcium stores. Also, physiological loads directly activate mechanoreceptors of the cell membrane like integrin, which actuate PKC (protein kinase C) and MAPK (mitogen activated protein kinase) signaling pathways. These signaling cascade propagates towards the nucleus, where it interacts with 51

	<i>mechanosensitive transcription factor and results in gene transcription.</i>	
Fig. 2.9	: <i>Intra-articularly injected HA-40 wt.% BaTiO₃ particulate in the knee joint of mice could not cause any systematic toxicity in vital organs, such as heart, kidney, liver and lung at 7 days of post-injection, as evident from representative fluorescent images.</i>	57
Fig. 3.1	: <i>Flow chart for the synthesis of Na_xK_(1-x)NbO₃ (x = 0.2, 0.5 and 0.8).</i>	104
Fig. 3.2	: <i>Digital images of (a) Conventional press, (b) Green pellets, (c) Cold isostatic press.</i>	105
Fig. 3.3	: <i>Surface charge polarization and measurement of thermally stimulated depolarized current. (a) Schematic illustration of high voltage (25 kV) corona poling unit for the development of electrical charges on the surface of the specimen. (b) Schematic shows the thermally stimulated depolarized current measurement setup includes picoammeter, furnace and simulator.</i>	110
Fig. 3.4	: <i>Schematic demonstrating the synergistic action of surface charge polarization and external electrical stimulation during cell culture experiment. The application of dynamic electrical stimulation (1 V/cm, 400 μs), while cells are being adhered on the (c) Neg. Pol. (d) Pos. Pol. surfaces.</i>	112
Fig. 3.5	: <i>Demonstration of intra-articular injection of NKN nanoparticles in the knee (synovial) joint of Wistar rat.</i>	122
Fig. 3.6	: <i>Schematic illustration of in vivo studies performed after intra-articular injection of Na_xK_{1-x}NbO₃ nanoparticles for 7 days. The histological analysis was done for the heart, liver, kidney, spleen and knee joint to for the inspection of microscopic changes in such organs. The inflammatory cytokines were examined on liver and spleen tissues to observe the level of inflammation after particulate injection. The blood serum extracted from the rats was used for biochemical assays (ALP and Creatinine) to analyze the cellular metabolism.</i>	123
Fig. 4.1	: <i>XRD patterns of the sintered HA and Na_xK_{1-x}NbO₃ (x = 0.2, 0.5 and 0.8) samples, (b) Positions of the most intense diffraction peaks (2 θ_M) in Na_xK_{1-x}NbO₃ (x = 0.2, 0.5 and 0.8).</i>	133
Fig. 4.2	: <i>Rietveld refinement analyses for NKN samples. The combined X-ray diffraction spectra for sintered Na_xK_{1-x}NbO₃ (x = 0.2 - 0.8) samples. Enlarged view demonstrating the observed and</i>	134

refined data for $x = 0.2, 0.5$ and 0.8 are illustrated.

- Fig. 4.3 : 4.3. X-ray peak profile analyses for $\text{Na}_x\text{K}_{1-x}\text{NbO}_3$ ($x = 0.2, 0.5, 0.8$) samples. Representation of plots obtained from (a) Modified Scherrer, (b) Williamson-Hall, and (c) Size-strain methods for $\text{Na}_x\text{K}_{1-x}\text{NbO}_3$ samples. 138
- Fig. 4.4 : FTIR spectra of the sintered HA and $\text{Na}_x\text{K}_{1-x}\text{NbO}_3$ ($x = 0.2, 0.5$ and 0.8) samples. 139
- Fig. 4.5 : Scanning electron microscopy (SEM) images and EDS graphs for $\text{Na}_x\text{K}_{1-x}\text{NbO}_3$ powders, (a) $x = 0.2$, (b) $x = 0.5$, (c) $x = 0.8$, calcined at 900°C for 10 h. 140
- Fig. 4.6 : Scanning electron microscopy (SEM) images and EDS graphs for fractured $\text{Na}_x\text{K}_{1-x}\text{NbO}_3$ samples, (a) $x = 0.2$, (b) $x = 0.5$, (c) $x = 0.8$, sintered at $1010, 1075$ and 1120°C , respectively. 140
- Fig. 4.7 : Mechanical properties of $\text{Na}_x\text{K}_{1-x}\text{NbO}_3$ ($x = 0.2, 0.5, 0.8$) and HA samples. Hardness and compressive strength of sintered specimens of $\text{Na}_x\text{K}_{1-x}\text{NbO}_3$ and HA. 142
- Fig. 4.8 : Na^+ and K^+ leaching profiles from $\text{Na}_{0.2}\text{K}_{0.8}\text{NbO}_3$ ($x = 0.2, 0.5, 0.8$) in SBF. The plot represents the dynamic changes in concentrations of Na^+ and K^+ , after immersion of $\text{Na}_x\text{K}_{1-x}\text{NbO}_3$ samples in SBF. 143
- Fig. 4.9 : Thermally stimulated depolarization current (TSDC) measurement. TSDC spectra of for $\text{Na}_x\text{K}_{1-x}\text{NbO}_3$ ($x = 0.2, 0.5, 0.8$) ceramics, polarized at 25 kV , followed by depolarization at the heating rate of $5^\circ\text{C}/\text{min}$. upto 500°C . 144
- Fig. 4.10 : XPS spectra for non-Pol. and polarized surfaces of NKN. (a) XPS survey spectrum of non-Pol. and polarized NKN for Na ($1s$), K ($2p$), Nb ($3p$), Nb ($3d$), C ($1s$) and O ($1s$) orbitals states. (b) and (c) represent the O $1s$ XPS spectra for non-Pol. and polarized NKN samples, respectively. 146
- Fig. 4.11 : Influence of surface polarization charge on hydrophilicity. The contact angle ($^\circ$) values for non-Pol. and polarized surfaces of $\text{Na}_x\text{K}_{1-x}\text{NbO}_3$ ($x = 0.2, 0.5, 0.8$) and HA in (a) DI water and (b) DMEM media. 148
- Fig. 4.12 : Influence of polarization on early-stage adhesion (after 6h) of MG-63 cells. (a) The representative florescence images of MG-63 cells, adhered on non-Pol. and polarized $\text{Na}_x\text{K}_{1-x}\text{NbO}_3$ and control samples. (b) The plot, representing the projected area of the adhered cells ($n = 20$), on the non-Pol. and polarized NKN and control samples. 150

- Fig. 4.13 : Quantitative cellular response on non-treated and treated NKN and control samples. The plots representing the quantitative cellular response, using (a) MG-63 cells and (b) hMSCs, on non-Pol. and polarized $\text{Na}_x\text{K}_{1-x}\text{NbO}_3$ ($x = 0.2, 0.5, 0.8$) and control samples in presence and absence of dynamic pulsed electrical stimulation. 154
- Fig. 4.14 : Osteogenic differentiation response of non-treated and treated piezoelectric NKN and control samples. The plot illustrating the alkaline phosphatase (ALP) activity on the non-Pol., electrostatically (Pos. and Neg. Pol.) – electrically stimulated (dynamic) Pos. Pol. (E. S. Pos.) and electrically stimulated (dynamic) Neg. Pol. (E. S. Neg.) $\text{Na}_x\text{K}_{1-x}\text{NbO}_3$ ($x = 0.2, 0.5, 0.8$) and HA samples, after (a) 7 and (b) 14 days. 157
- Fig. 4.15 : Morphological analyses of adhered cells on non-treated and treated NKN and control samples. (a) Representative fluorescence microscopic images of stained hMSCs, adhered on the non-treated and treated (Electrostatically/dynamically stimulated) piezoelectric $\text{Na}_x\text{K}_{1-x}\text{NbO}_3$ samples and control. 159
- Fig. 4.16 : The level of intracellular Ca^{2+} on non-treated and treated NKN and control samples, cultured with MG-63 cells. The plot representing the mean of the peak values of the ratio of fluorescence intensity at 340 and 380 nm, measured for the cells loaded with intracellular Ca^{2+} indicator Fura-2 AM on the non-treated and treated (Electrostatically/dynamically stimulated) piezoelectric $\text{Na}_x\text{K}_{1-x}\text{NbO}_3$ samples and control. 161
- Fig. 4.17 : Schematic demonstrating the synergized effect of Neg. Pol. surface and dynamic pulsed electrical stimulation in promoting cellular response of piezoelectric NKN. 164
- Fig. 5.1 : Quantitative analyses of antibacterial response on the non-polarized and polarized surfaces of $\text{Na}_x\text{K}_{1-x}\text{NbO}_3$ ($x = 0.2 - 0.8$) and HA samples for (a) *S. aureus* and (b) *E. coli* bacteria. 175
- Fig. 5.2 : Antibacterial ratio % (calculated from eqn. 3.5, chapter 3) for the non-polarized and polarized surfaces of $\text{Na}_x\text{K}_{1-x}\text{NbO}_3$ ($x = 0.2 - 0.8$) and HA samples with (a) *S. aureus* and (b) *E. coli* bacteria. 177
- Fig. 5.3 : Florescence microscopy images representing the live and dead strain of (a) *S. aureus* and (b) *E. coli* bacteria, exposed on non-polarized and polarized $\text{Na}_x\text{K}_{1-x}\text{NbO}_3$ ($x = 0.2 - 0.8$) and HA samples after 10 h of incubation in growth medium. Live and dead bacteria are strained green and red, respectively. Scale bar = 25 μm . 178

- Fig. 5.4 : Digital camera images of (A) *S. aureus* and (C) *E. coli* bacterial colonies on agar plate exposed with non-polarized and polarized $\text{Na}_x\text{K}_{1-x}\text{NbO}_3$ ($x = 0.2 - 0.8$) and HA samples. 181
- Fig. 5.5 : The plots illustrating the concentration of superoxide ($\bullet\text{O}_2^-$) on non-polarized and polarized $\text{Na}_x\text{K}_{1-x}\text{NbO}_3$ ($x = 0.2 - 0.8$) as well as HA samples for (a) *S. aureus* and (b) *E. coli* bacteria. 184
- Fig. 5.6 : The plots representing the catalase activity/ seconds on non-polarized and polarized $\text{Na}_x\text{K}_{1-x}\text{NbO}_3$ ($x = 0.2 - 0.8$) as well as HA samples for (a) *S. aureus* and (b) *E. coli* bacteria. 186
- Fig. 5.7 : The plots representing the leaked amount ($n \text{ mol/ mg}$), of intracellular bacterial protein for (a) *S. aureus* and (b) *E. coli* bacteria on non-polarized and polarized $\text{Na}_x\text{K}_{1-x}\text{NbO}_3$ ($x = 0.2 - 0.8$) and HA samples. 189
- Fig. 5.8 : The plots representing the MDA concentration (nmol./mg) (calculated from eqn. 5.2) for (a) *S. aureus* and (b) *E. coli* bacteria, cultured on non-polarized and polarized $\text{Na}_x\text{K}_{1-x}\text{NbO}_3$ ($x = 0.2 - 0.8$) and HA samples. 192
- Fig. 5.9 : Schematic representing various mechanisms of antibacterial response of NKN samples, induced by surface charge polarization 195
- Fig. 6.1 : X-ray diffraction pattern of micro-sized and nano-sized (after 10 h planetary ball milling) $\text{Na}_x\text{K}_{1-x}\text{NbO}_3$ ($x = 0.2 - 0.8$) powders. Enlarged view illustrating the position and intensity of most intense diffraction peaks of NKN samples before and after ball milling. (B. M: Planetary ball milling). 201
- Fig. 6.2 : High resolution scanning electron microscopy (HRSEM) images and EDS graphs for $\text{Na}_x\text{K}_{1-x}\text{NbO}_3$ nano-powders, (a) $x = 0.2$, (b) 0.5, (c) 0.8, planetary ball milled for 10 h. 203
- Fig. 6.3 : (A) Qualitative and (B) quantitative response of MG-63 cells after 24 and 72 h of culture on $\text{Na}_x\text{K}_{1-x}\text{NbO}_3$ ($x = 0.2, 0.5, 0.8$) nanopowders i.e., N1, N2, N3 of concentrations, C1 (0.25 mg/ml), C2 (2.5 mg/ml) and C3 (25 mg/ml). Scale bar = 100 μm . 205
- Fig. 6.4 : Representation of the paws of the rats before and 7th days' post intra-articular injection of NKN nanoparticulates and the knee joint, confirming the absence of any inflammation. 207
- Fig. 6.5 : Effect of intra-articular injection of N1, N2, and N3 compounds on body weight of the rats during the experimental protocol. All values are represented as mean \pm SD ($n = 6$ rats/group) (Two- 208

way ANOVA followed by Bonferroni post hoc test).

- Fig. 6.6 *Effect of intra-articular injection of N1, N2, and N3 compounds on serum concentration of (a) Alkaline phosphatase activity (ALP) and (b) Creatinine, at the end of day 7 of the experimental protocol.* 210
- Fig. 6.7 : *The plots representing the percentage of fold change (w. r. t. GAPDH) in gene expression of proinflammatory (TNF- α and IL-12) and anti-inflammatory (IL-4 and IL-10) cytokines for N1, N2, N3 treated, saline treated and control (non-injected) rats in (a) liver and (b) spleen.* 212
- Fig. 6.8 : *Histopathological images of hematoxylin and eosin (H & E) stained heart tissues of (a) Control (non-injected), (b) Saline, (c) N1, (d) N2 and (e) N3 nanoparticulate eluates treated groups of rats after 7 days of intra-articular injection.* 214
- Fig. 6.9 : *Histopathological images of H & E stained liver tissues of (a) Control (non-injected), (b) Saline, (c) N1, (d) N2 and (e) N3 nanoparticulate eluates treated groups of rats after 7 days of intra-articular injection.* 216
- Fig. 6.10 : *Histopathological images of H & E stained kidney tissues of (a) Control (non-injected), (b) Saline, (c) N1, (d) N2 and (e) N3 nanoparticulate eluates treated groups of rats after 7 days of intra-articular injection.* 218
- Fig. 6.11: *Histopathological images of H & E stained spleen tissues of (a) Control (non-injected), (b) Saline, (c) N1, (d) N2 and (e) N3 nanoparticulate eluates treated groups of rats after 7 days of intra-articular injection.* 220
- Fig. 6.12 : *Histopathological images of H & E stained knee joint tissues of (a) Control (non-injected), (b) Saline, (c) N1, (d) N2 and (e) N3 nanoparticulate eluates treated groups of rats after 7 days of intra-articular injection. NKN treated knee joint tissues are showing smooth cartilage with the deposition of particles.* 223

List of Tables

Table 2.1	<i>A comparison of dielectric constants (ϵ_r), piezoelectric strain coefficients (d_{33}), mechanical quality factors (Q_m), remnant polarization (P_r), electromechanical coupling coefficients (k_p) and pyroelectric coefficients (p) of various piezoelectric biomaterials with those of the natural bone.</i>	26
Table 2.2	<i>Table 2.2. Effect of various processing techniques on densification ($\% \rho_{th}$), piezoelectric strain coefficient (d_{33}) and electromechanical coupling coefficient (k_p) of the NKN/ NKN-based ceramics.</i>	41
Table 2.3	<i>Table 2.3. Effect of doping on densification, piezoelectric (d_{33}) and dielectric (ϵ_r) properties of NKN.</i>	45
Table 3.1	<i>Sintering parameters, optimized for the developed compositions.</i>	106
Table 4.1	<i>Table 4.1. The refined unit cell parameters and the positions of most intense diffraction peak ($2\theta_M$) for the $Na_xK_{1-x}NbO_3$ ($x = 0.2, 0.5$ and 0.8) samples.</i>	133
Table 4.2	<i>The final obtained values of various refined parameters, corresponding to monoclinic phases in $Na_xK_{1-x}NbO_3$ ($x = 0.2, 0.5, 0.8$) samples, sintered at 1010, 1075 and 1120 °C, respectively.</i>	135
Table 4.3	<i>Geometrical parameters of solid state synthesized $Na_xK_{1-x}NbO_3$ ($x = 0.2, 0.5, 0.8$) samples, sintered at 1010, 1075 and 1120 °C, respectively.</i>	137